Mechatronics 61 (2019) 69–82

Contents lists available at ScienceDirect

Mechatronics

journal homepage: www.elsevier.com/locate/mechatronics

A novel hand exoskeleton with series elastic actuation for modulated torque transfer ☆

Dario Marconi [a,1,*], Andrea Baldoni [a,1], Zach McKinney [a], Marco Cempini [a,2], Simona Crea [a,b], Nicola Vitiello [a,b]

[a] The BioRobotics Institute, Scuola Superiore Sant'Anna, Pisa, Italy
[b] Fondazione Don Gnocchi, Milan, Italy

ARTICLE INFO

Keywords:
Hand exoskeleton
Series elastic actuators
Wearable assistive technology
Thumb opposition
Stroke
Robotic rehabilitation

ABSTRACT

Among wearable robotic devices, hand exoskeletons present an important and persistent challenge due to the compact dimensions and kinematic complexity of the human hand. To address these challenges, this paper introduces HandeXos-Beta (HX-β), a novel index finger-thumb exoskeleton for hand rehabilitation. The HX-β system features an innovative kinematic architecture that allows independent actuation of thumb flexion/extension and circumduction (opposition), thus enabling a variety of naturalistic and functional grip configurations. Furthermore, HX-β features a novel series-elastic actuators (SEA) architecture that directly measures externally transferred torque in real-time, and thus enables both position- and torque-controlled modes of operation, allowing implementation of both robot-in-charge and user-in-charge exercise paradigms. Finally, HX-β's adjustable orthosis, passive degrees of freedom, and under-actuated control scheme allow for optimal comfort, robot-user joint alignment, and flexible actuation for users of various hand sizes. In addition to the mechatronic design and resulting functional capabilities of HX-β, this work presents a series of physical performance characterizations, including the position- and torque-control system performance, frequency response, end effector force, and output impedance. By each measure, the HX-β exhibited performance comparable or superior to previously reported hand exoskeletons, including position and torque step response times on the order of 0.3 s, −3 dB cut-off frequencies ranging from approximately 2.5 to 4 Hz, and fingertip output forces on the order of 4 N. During use by a healthy subject in torque-controlled transparent mode, the HX-β orthosis joints exhibited appropriately low output impedance, ranging from 0.42 to −0.042 Nm/rad at 1 Hz, over a range of functional grasps performed at real-life speeds. This combination of lab bench characterizations and functional evaluation provides a comprehensive verification of the design and performance of the HandeXos Beta exoskeleton, and its suitability for clinical application in hand rehabilitation.

1. Introduction

1.1. Hand exoskeletons in neurorehabilitation

In recent years, an increasing number of wearable robotic exoskeletons have been developed and investigated for various applications in movement augmentation and neuro-motor rehabilitation [1–3]. Due to their capacity to provide precise, repeatable, and adaptive movement assistance, exoskeletal robots have demonstrated extensive feasibility and clinical potential in assisting physical therapists and physicians to conduct neurorehabilitation exercises [4–9]. In addition to smart and adaptive movement assistance, rehabilitation robotics offer a reliable quantitative method for functional performance assessment, by measuring kinetic movement parameters such as speed, joint torques, and range of motion.

These capabilities are especially pertinent to the rehabilitation of hand function, which is commonly required following a variety of neurological injuries including stroke, traumatic brain injury, and spinal cord injury, as well as peripheral nerve injuries and neuropathies [10–14]. The recovery of dexterous or semi-dexterous hand function is clinically significant because it is essential to individual autonomy with respect to both vocation and activities of daily living. Indeed, hand function has been identified as the leading quality-of-life-related priority by individ-

☆ This work was supported in part by the Regione Toscana under the RONDA project (BANDO FAR-FAS Salute 2014) and the Italian Institute for Accidents at Work (INAIL) under the HABILIS project.

* Corresponding author.
E-mail address: dario.marconi@santannapisa.it (D. Marconi).

[1] These authors are equal contributors.
[2] When the activities described in this paper were carried out.

https://doi.org/10.1016/j.mechatronics.2019.06.001
Received 26 November 2018; Received in revised form 14 May 2019; Accepted 2 June 2019
Available online 18 June 2019

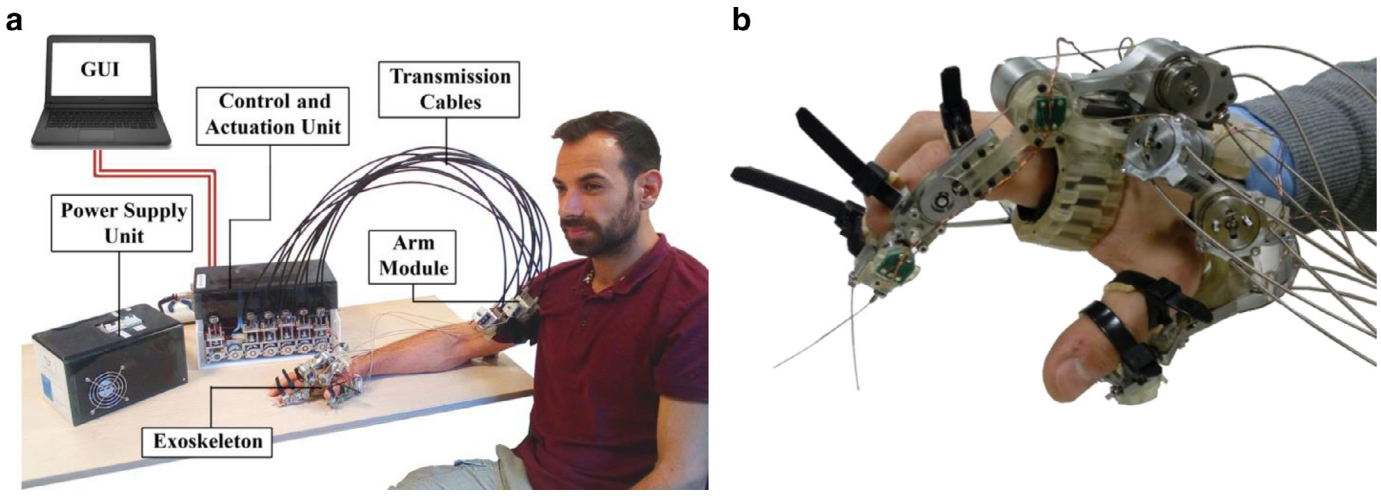

Fig. 1. (a) System-level view of the HandeXos-β (HX-β) system. Red line to graphical user interface (GUI) represents wired connection; (b) Close-up view of the HX-β orthosis (exoskeleton).

uals with quadriplegia due to spinal cord injury - above walking, bowel, bladder, and sexual function [15].

Due to the required dexterity and precision of motion assistance relative to what can be manually provided by a physical therapist, hand rehabilitation may be greatly enhanced by the use of wearable robotic devices. In particular, hand exoskeletons offer the capacity to provide simultaneous, targeted, multi-joint assistance in achieving precise grasping configurations of high functional utility [4,5,16].

However, the compact dimensions and kinematic complexity of the hand have posed a formidable design challenge to the development of effective hand exoskeletons for rehabilitation applications to date. As discussed further in Section 1.2, traditional rigid-frame hand exoskeletons have been limited by three major shortcomings: their kinematic mismatch with the human hand, their rigid position-based control schemes, and their cumbersome, uncomfortable ergonomics. By contrast, soft exoskeletons are usually lighter, more comfortable, and easier to wear [17–20], but pose a number of separate drawbacks related to their limited sensing and control capabilities, since the lack of rigid frames renders their kinematics indeterminate.

This paper introduces a novel powered hand exoskeleton called HandeXos-Beta (HX-β) (Fig. 1) that addresses each of these challenges and limitations of previous devices. Based on the design of the original HandeXos (HX) [21] developed at The BioRobotics Institute of Scuola Superiore Sant'Anna (Pisa, Italy), HX-β implements an innovative and naturalistic kinematic architecture, a series-elastic actuator (SEA) architecture capable of both position- and torque-controlled modes, and an adjustable, ergonomic robotic orthosis. In addition to the mechatronic description of the HX-β exoskeleton, this work presents a series of experimental characterizations of HX-β performance. The detailed design of HX-β system is described in Section 2, followed by the methods of performance characterization in Section 3. Results of the experimental characterization are reported in Section 4 and discussed in Section 5, followed by conclusions in Section 6.

1.2. Technical and functional requirements

In the field of rehabilitation robotics, the kinematic compatibility, fit, and comfort of robotic orthoses are among the design aspects most crucial to ensure the safety, effectiveness, and clinical usability of exoskeletal devices. Due to the highly constrained, joint-by-joint interactions between the robot and the user (characteristic of wearable robotics in general), the orthosis must achieve and maintain good alignment between the robotic and human joint axes to optimize comfort and avoid undesired parasitic forces on the skeletal system. Indeed, even small misalignments between the robotic and physiological rotation axes can result in unnatural and undesired translational forces at the human-robot interface, which can significantly diminish both the comfort and the effectiveness of the device [22].

Achieving satisfactory joint alignment is especially challenging for hand exoskeletons, owing to both the spatial constraints and kinematic complexity of the human hand. With its capacity for compound, multi-degree-of-freedom (DOF) movements, the hand often employs functional (i.e. effective) axes of rotation displaced and/or misaligned with anatomical joint axes, and it is these functional axes with which the robot must align for optimal comfort and fidelity of control [7,21]. However, the precise location and orientation of physiological joints (both anatomical and functional) is often impossible to identify without complex imaging techniques and geometrical analysis. In practice, achieving adequate robot-user alignment often requires robotic systems to employ remote centers of motion, when direct physical alignment with anatomical joints is not possible due to spatial constraints [23].

With respect to control schemes, a core principle of robotically assisted rehabilitation is that exoskeletal devices should work safely and collaboratively with the user (patient), by seeking to exploit and enhance the user's residual capabilities [4]. Consequently, the actuation and control systems of hand exoskeletons should enable at least two distinct modes of operation: a position-controlled "robot-in-charge" mode [24], and a torque-controlled "patient in charge" mode [13,25]. In robot-in-charge mode, the robot moves along pre-defined spatio-temporal trajectories, defined and/or modulated by the clinician. This mode is necessary for patients with high degrees of muscle tonicity (spasticity) and/or motor impairment, to mobilize the hand and train desired grasping patterns. For users with moderate-to-advanced functional capabilities, a torque-controlled "patient-in-charge" mode is warranted, in which the user retains primary control and the robot offers variable levels of assistance, only as necessary to complete the desired task(s).

To implement this torque-controlled mode effectively, exoskeletons must have precise real-time measurement of the external torques (and/or forces) transferred from the robot to the user. However, traditional robotic systems have been limited in their capacity to measure this external torque, due to their reliance on actuator-embedded sensors that cannot account for downstream frictional losses in the transmission and/or kinematic chain. A common mechanism that has been developed to solve this problem in exoskeletal robotics has been the series-elastic actuator (SEA), which can measure external torques directly, by means of a torsional spring coupled directly to the user's joint, in series with the joint actuator (motor) [26]. In such systems, the instantaneous ex-

ternal joint torque is obtained from the product of the SEA's torsional spring deformation (measured with one or more angular encoders) and the known spring constant.

However, due to the additional spatial encumbrance of the series spring, which cannot be displaced from the user's joint in the same fashion as remote (e.g. cable-driven) actuation systems and must instead be deployed directly at or immediately adjacent to the point of action, few SEAs have been implemented in hand exoskeletons [27]. As an alternative approach, an optical linear force sensor has recently been integrated into the distal link of a hand exoskeleton for rehabilitation, for direct measurement of human-robot interaction forces [28]. While the force-sensing performance of this system was sufficient to enable a force-triggered control scheme and a continuously controlled low-impedance mode, the design relies on the collective rigidity of the kinematic chain and thus offers neither the desired elasticity of the SEA architecture, nor the ability to maintain dynamic robot-user joint alignment via passive degrees of freedom.

Finally, in order to achieve adequate comfort during prolonged use (such as in an extended physiotherapy session), the robotic components making direct contact with the user should have an ergonomic geometry and employ compliant materials at the point of contact. By contrast, the human-robot interface of the original HX exoskeleton was composed of a series of metal cuffs, ensuring a very reliable interaction, but in turn presenting some drawbacks with respect to comfort [21]. In particular, the HX orthosis could not be adjusted to fit hands of different sizes, thus greatly reducing the range of possible users. Moreover, the stiff metal interface occasionally proved to be uncomfortable during extended use, especially by impaired individuals. The HX-β includes a novel set of mechanisms and features that address each of the above deficits, as further described below.

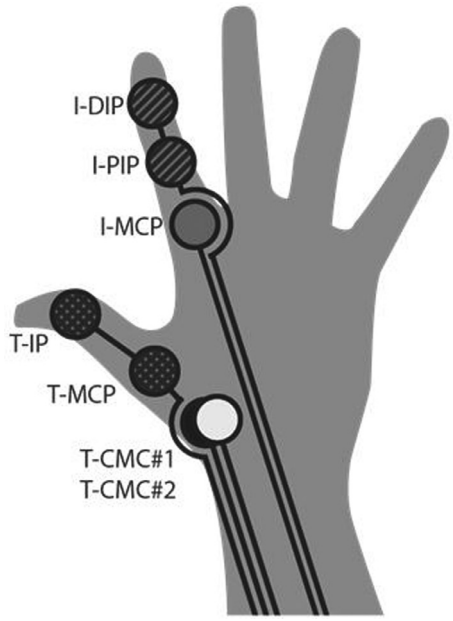

Fig. 2. Mapping of HandeXos-β's five SEA actuation units to their corresponding hand joints: index metacarpo-phalangeal (I-MCP, grey), index proximal inter-phalangeal and index distal inter-phalangeal (I-PIP, I-DIP, single-hatch), thumb carpo-metacarpal #1 (T-CMC#1,white), thumb carpo-metacarpal #2 (T-CMC#2, black), thumb metacarpo-phalangeal and thumb inter-phalangeal (T-MCP, T-IP, cross-hatch). I-PIP and I-DIP are under-actuated and together are named I-IP, T-MCP and T-IP are under-actuated and together are named (T-MCPIP).

2. Materials and methods

This section provides a detailed technical description of the HandeXos Beta (HX-β) robotic hand exoskeleton system, beginning with a system-level overview (Section 2.1) and summary of new and novel features (Section 2.2), including the novel palm-thumb kinematic chain (Section 2.2.1), series elastic actuator (SEA) architecture (Section 2.2.2), and ergonomic enhancements relative to the predecessor HandeXos device (2.2.3). Next, a detailed mechatronic characterization is provided, including the HX-β hardware (Section 2.3), thumb kinematics (Section 2.4), and control architecture (Section 2.5). Finally, the methods used for performance characterization of the index finger are detailed in Section 2.6.

2.1. HandeXos Beta system architecture overview

HX-β (Fig. 1) is a cable-driven index finger-thumb exoskeleton consisting of a robotic hand orthosis, upper arm coupling module, and two bench-top units – one for control and remote actuation, and the other for power supply. The HX-β system features a total of five bi-directional series-elastic actuation (SEA) units, controlling seven degrees of freedom (DOF), including both fully and under-actuated DOF, as summarized in Fig. 2. Specifically, the index metacarpophalangeal (MCP) joint (providing index flexion-extension) and the two carpo-metacarpal (T-CMC) joints of the thumb (combining to provide thumb circumduction and opposition) are fully actuated by dedicated SEAs. By contrast, the two distal joints of each digit (index proximal and distal IP joints, and thumb IP + MCP) are under-actuated, with each joint pair controlled in tandem by a single SEA.

For both the fully and under-actuated DOF, each SEA unit is spatially distributed, comprising an elastic-encoder module (EEM: torsional spring + encoder) incorporated directly into the hand orthosis, and the corresponding actuator (motor) residing in the bench-top control and actuation unit. Each actuator is coupled to its respective EEM by a two-stage Bowden cable transmission, with each stage consisting of an antagonistic cable pair.

The two stages of cable transmission are coupled in the upper arm module, which maintains the distal span of fine-gauge Bowden cable that directly drives orthosis in a clean, kink-free configuration (to minimize frictional disturbances in the transmission line) and allows for practical setup and easy re-positioning of the user in a clinical setting. In addition to the primary kinematic structure, the HX-β orthosis (Fig. 1b) features a variety of integrated size adjustment mechanisms.

2.2. Summary of innovations and design improvements

HandeXos Beta offers three primary innovations with respect to existing exoskeletons, including its predecessor (HX):

1) An improved kinematic architecture, featuring a novel thumb kinematic chain that allows for better alignment of the human and robot joint axes, as well as a remote center of motion coinciding with the hand's carpal-metacarpal (CMC) joint. Additional passive degrees of freedom have also been added for better joint alignment, to further improve the human-robot kinematic compatibility.
2) A series elastic actuator (SEA) architecture, featuring integrated position and torque sensors, which allow for the implementation of both position- and torque-based control modes, for robot- and patient-in-charge protocols, respectively.
3) A comfortable and adjustable robotic orthosis, allowing for a better fit with proper robot-hand joint alignment across a wider range of users.

2.2.1. Kinematic chain improvements

In order to achieve good robot-user joint alignment and naturalistic patterns of articulation, the HX-β improves upon the HX architecture with three significant developments. First, HX-β incorporates a novel thumb kinematic chain, comprising two actuated joints (Fig. 3b, joints

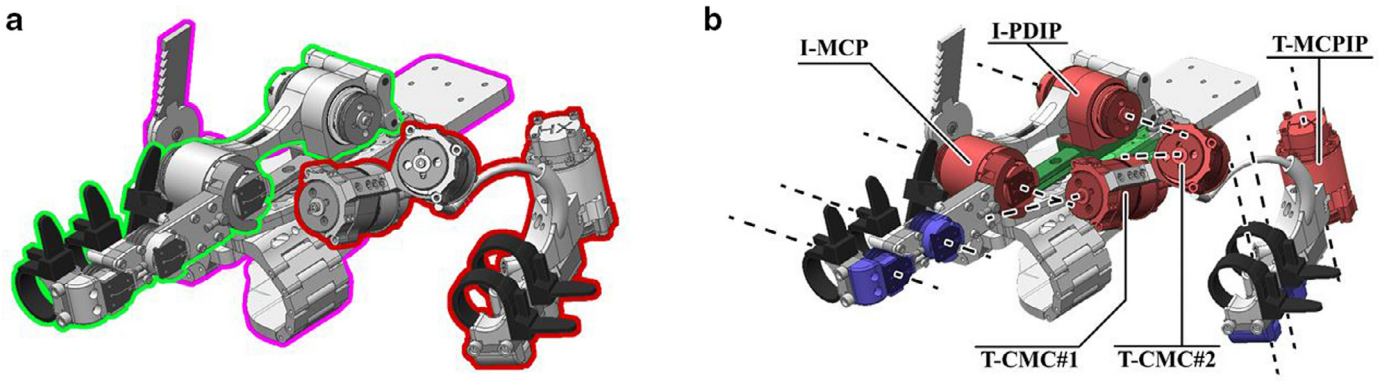

Fig. 3. a) Differentiation of thumb (red) and index (green) kinematic chains, as well as the palm-mounted base module (purple); b) Differentiation of joint types: SEA-EEM units (red – 5 total), under-actuated joints with integrated angle encoders (purple – 4 total), and passive DOF (green).(For interpretation of the references to colour in this figure legend, the reader is referred to the web version of this article.)

T-CMC #1 and #2) with incident axes designed to coincide with CMC joint of the hand. Working in concert, these two joint axes combine to enable rotation about an intermediate virtual axis corresponding to the natural axis of thumb circumduction, a functionally significant form of thumb opposition that combines flexion/extension (F/E) and adduction/abduction in a (roughly) circular arc [29–31]. In addition to serving as a form of active thumb opposition for grips such as the lateral "key pinch" grip, circumduction allows for grip re-configuration, to apply F/E in different planes – for instance, to transition from a lateral pinch to a precision pinch or power grip. Anatomically, thumb circumduction is achieved by coordinated activity of the CMC, MCP, and IP joints [29]. The palm-thumb kinematics of HX-β are described in full mechatronic detail in Section 2.5.

In addition to the novel thumb kinematic chain, HX-β builds upon the HX architecture by implementing two additional passive degrees of freedom (pDOF) to allow for dynamic self-alignment of the orthosis with the user's anatomy during use – one for the internal/external rotation of the index finger, and one for the internal/external rotation of the thumb.

2.2.2. Series elastic actuator (SEA) architecture

A series elastic actuation (SEA) architecture was developed and incorporated into the HX-β system to allow the implementation of a torque-control mode, thus enabling HX-β to provide variable assistance on an as-needed basis. The SEA architecture is distributed between the hand orthosis and the remote actuation unit, as described above, in Section 2.1. In order to measure the externally transferred torque as directly as possible, elastic-encoder modules (EEMs) consisting of torsional spring elements [32] and their corresponding encoders are incorporated into the joints of the HX-β orthosis for each of the five active DOFs (Fig. 3b).

For the three fully actuated DOFs (index MCP and both thumb CMCs), the EEM is incorporated directly into the corresponding robotic joint, with co-axial alignment between the joint and the EEM's torsional spring. For the under-actuated joints (index IP and thumb IP + MCP), the corresponding EEM is displaced from the joint axes by the minimum feasible distance given the spatial constraints of the hand, and coupled with the joints by a short span of uninsulated cable.

A detailed view of the EEM architecture is provided in Fig. 4. Each EEM consists of a custom-designed torsional spring and a magnetic absolute position encoder (Ref: AS5410, AMS, Premstaetten, Austria). The springs exhibit a linear torque-deformation behavior, with a constant stiffness of 1.34 N·m/rad and maximum deflection of about ±20°, which corresponds to about ±0.6 N·m. The encoders are connected to a custom printed circuitboard and coupled with a diametric magnet mounted on the input shaft of the springs, at a distance of 1 mm from the center of rotation. The encoders provide a direct measurement of the spring deformations, which in turn allow calculation of the external torques exerted on the joints [33].

2.2.3. Human-robot interface ergonomics

The HX-β orthosis features a series of design enhancements to overcome the ergonomic limitations of the preceding HX exoskeleton described in Section 1.2 – namely:

- *Robotic adjustment mechanism*: Each digit of the HX-β exoskeleton features an adjustment mechanism that can be used to increase or decrease the joint segment lengths, thus enabling better alignment between the robotic and human joints. Further, the thumb module features a setscrew-based mechanism to adjust the default abduction/adduction (A/A) angle (Fig. 4).
- *Adjustable palm strap*: The strap around the user's palm is composed of a series of segments. The strap can be elongated or shortened to better accommodate different users by simply adding or removing segments (Fig. 4).
- *Adjustable finger straps*: The phalanges of the exoskeleton are equipped with adjustable straps that can be tightened around the user's finger, for a snug yet comfortable fit. The straps are internally coated with a layer of soft fabric, to further improve comfort and avoid skin abrasion.

2.2.4. HandeXos Beta mechatronic architecture–hardware

HandeXos Beta (HX-β) is a thumb-index hand exoskeleton designed for rehabilitation and assistance of both neurological and traumatic impairment of the right hand. Similarly to the original HX device [21], HX-β is composed of two fingers (index and thumb), with a total of seven revolute joints distributed along the physiological kinematic chain. Like the human hand, HX-β is remotely actuated and cable -driven. This section provides a detailed component-level description of HX-β's various mechatronic modules (Fig. 3).

2.2.5. Actuation units

As summarized in Section 2.1, the HX-β actuation system (Fig. 1) is displaced remotely from the exoskeletal orthosis, to reduce the weight and encumbrance of the motors on the user's movement. The HX-β actuators consist of five 15 W bi-directional DC motors (Ref no. 236655, Maxon Motor, Sachseln, Switzerland), corresponding to the five active DOFs (Fig. 2): three fully actuated joints (I-MCP, T-CMC#1, and T-CMC#2) and two under-actuated joint pairs (I-IP and T-IP/MCP).

Each actuator is connected to a Bowden cable transmission system by way of a 132:1 reduction stage (Ref no. 166171, Maxon Motor, Sachseln, Germany) and a pair of leadscrews (0.7 mm/revolution) that drive the two ends of an antagonistic cable pair by equal amounts in opposite directions, to synchronize the pull of one cable with the relaxation of its

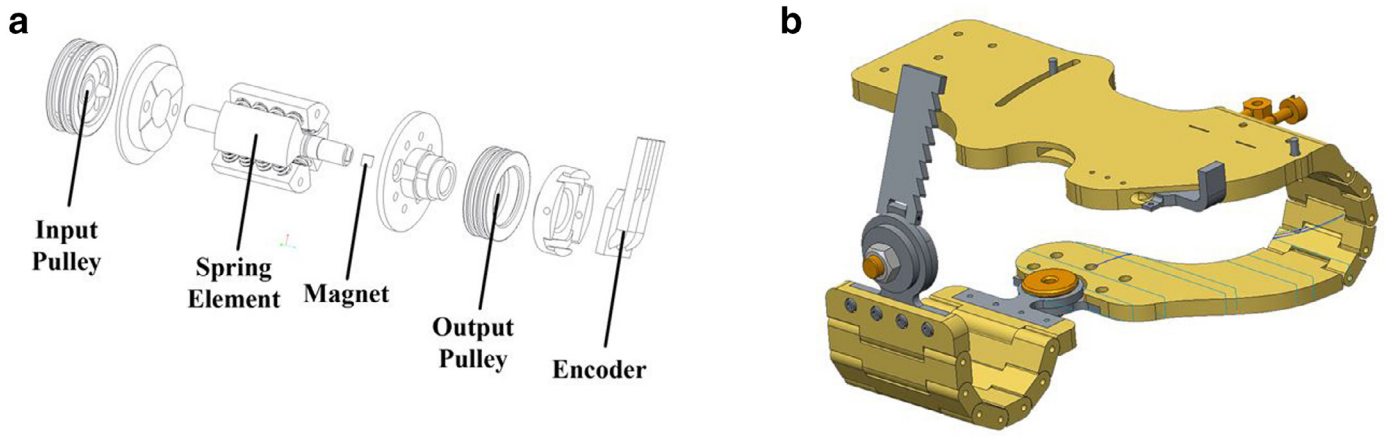

Fig. 4. (a) Expanded detail of HX-β elastic-encoder module (EEM), of the series-elastic actuation (SEA) architecture [32], (b) Palm-mounted base module, featuring adjustable palm strap.

antagonist. Finally, each actuator is equipped with an encoder (Ref no. 225783, Maxon Motor, Sachseln, Germany) that measures the angular position of the motor output shaft.

2.2.6. Cable transmission

Each of the five HX-β actuators is coupled directly (by leadscrew) to an antagonistic pair of Bowden cables, to effect flexion and extension movements of the exoskeleton. As introduced in Section 2.1 and illustrated in Fig. 1, the cable transmission consists of two stages: a proximal stage, extending from the actuator to a coupling module worn on the upper arm, and a distal stage, which directly drives each of the exoskeleton joints, via EEM. Both the proximal and distal cable transmissions consist of antagonistic pairs of Bowden cables, of different types. Both proximal and distal transmission cables consist of steel wires, with a respective diameters of 1.12 mm and 0.46 mm (Carl Stahl, Sussen, Germany), routed through flexible sheaths made of spiralized harmonic steel wire (Spin-Off Laboratory Company of Limited, Hokkaido, Japan), with outer/inner diameters of 6.0/2.5 mm and 1.6/0.8 mm, respectively.

The proximal and distal transmission cables are coupled in the upper arm module by a friction clutch-pulley system, in which the output pulley of the proximal transmission cables is coupled via friction clutch to the input pulley of the distal transmission cables. Finally, the displacement (tension) of the distal transmission cables is translated into joint articulation of the HX-β orthosis by rotary pulleys embedded in each of the EEM modules, which are rigidly coupled to the torque output segments of the orthosis (i.e. those in direct contact with the user's hand segments). The terminals of each distal cable are rigidly fixed to the EEM pulleys via leadscrew, which may be used to manually regulate cable pre-tension according to the user's hand size and natural resting hand position. For the under-actuated joints only, the rotation of the EEM pulley is further translated to the distal joints (I-IP and T-IP/MCP) by an additional cable-pulley transmission system described previously in [21].

2.3. HX-Beta mechatronic architecture-electronics

2.3.1. Sensors

All together, the HandeXos Beta system is equipped with a total of 14 sensors, including five encoders for torque measurement embedded in each of the elastic-encoder modules (EEMs) (AS5410 Hall Encoder, AMS AG), and the five output shaft position encoders embedded in the five actuator motors (MR Encoder, 256 CPT, 3 Channels, Maxon Motor). The last four encoders are embedded to record the position of the finger joints, but were not used in this study. Together, these sensors are used to effect the various levels of control described in Section 2.5, with the actuator motor encoders used to effect position control mode, and the EEM encoders used to effect torque control mode.

2.3.2. Control electronics

The HX-β control system consists of a real-time controller (Ref: NI-sbRIO-9626, National Instruments, TX, USA), featuring a real-time 400 MHz processor running a real-time NI operating system, and a field programmable gate array (FPGA) processor (Spartan 3, Xilinx). The control electronics are housed along with the HX actuators in a dedicated bench-top unit (Fig. 1).

2.3.3. Power supply unit

The HX-β power supply electronics are housed in a separate box, connected to the control electronics and actuation unit, and plugged to the power source (Fig. 1). This box contains two different power supplies: one 24 V/5A power supply (ABB CP-C 24/5.0 In:110–240VAC/100–350VDC Out:DC 24 V/5A) and one 24 V/2.5A power supply (SITOP PSU100S 24 V/2.5 A 6EP1332-2BA20). Moreover, the power supply unit contains a battery that makes the device portable when necessary (TopFuel LiPo 40C-POWER 6S/3900mAh, 22.2 V, 40C Dauer, # 83900671). Three switches control the power flow at different levels: a general switch (ABB M201-1A Magnetothermic), a second switch that enables the electronics, and the third switch that enables the motors (both Schneider electric C60HB-B116).

2.4. HX-Beta mechatronic architecture–palm-thumb kinematics

This section details the design and articulation of the HandeXos-Beta palm-thumb kinematic chain, which represents the primary innovation of the HX-β system with respect to kinematic design. In particular, we focus on the kinematics of the thumb base movement about the carpal-metacarpal (CMC) joint, as effected by the two dedicated series elastic actuation (SEA) units T-CMC #1 and T-CMC #2 (Figs. 2 and 3b). Aside from the incorporation of additional passive degrees of freedom and the implementation of SEA architecture in HX-β, the basic design and kinematics of the index chain and the distal thumb (MCP and IP joints) are as described the original HandeXos device [21], providing active flexion and extension of the IP and MCP joints.

2.4.1. Palm-thumb kinematic chain architecture

The palm-thumb kinematic chain (PTKC) is among the primary innovations of the HX-β device, enabling articulation of the thumb carpo-metacarpal (T-CMC) joint throughout its natural (healthy) range of motion in a variety of functionally relevant grip configurations. In particular, it allows the dynamic combination of F/E and circumduction movements, to achieve active opposition in a range of planes and configurations. Significantly, by creating a remote virtual axis via the compound

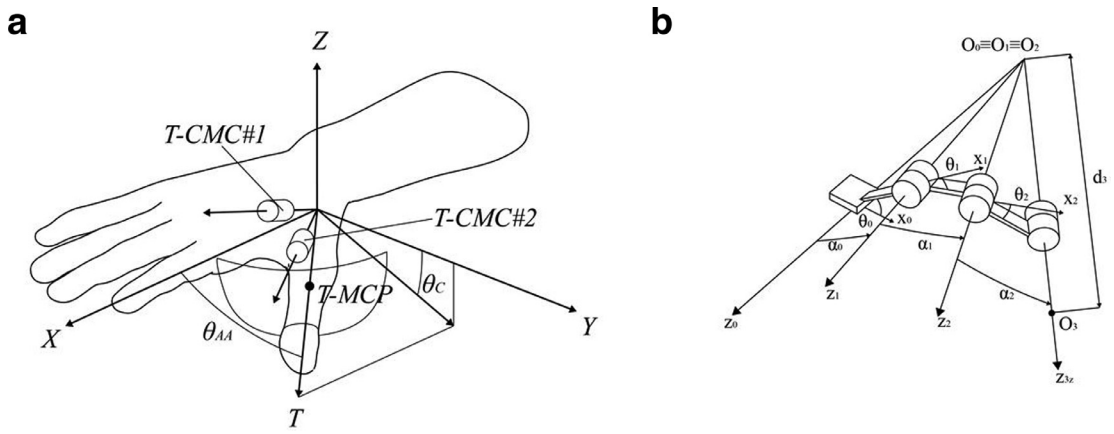

Fig. 5. (a) Workspace of Palm-Thumb Kinematic Chain, (b) Denavit-Hartenberg representation of the Palm-thumb kinematic chain.

movements of two robotic CMC joints working in synergy, the PTKC replicates the motion of the natural CMC joint without occupying the joint's anatomical space.

The PTKC (Fig. 3) is composed of three active revolute joints with SEA-EEM architecture (T-MCP/IP, T-CMC #1, T-CMC #2), with the T-MCP/IP actuation unit distributed in tandem to the T-MCP and T-IP joints, each containing their own embedded encoders.+ Among the three T-EEM joints, two (T-CMC #1 and #2) combine to effect thumb circumduction, while the third actuates the T-IP and T-MCP joints in underactuated fashion, to achieve thumb flexion and extension.

In addition to the active joints, the PTKC base features mechanisms for positioning and adjusting the kinematic chain to the user's anatomy. Specifically, the two active T-CMC joints (Fig. 3) are adjusted so that their axes remain intersecting within the anatomical thumb CMC joint. Kinematically, the "end effector" of the PTKC – namely, the T-MCP joint – serves as the base of the remaining thumb kinematic chain, consisting of the T-MCP and T-IP joints, which operate in F/E in the same way as the index chain. Accordingly, the T-MCP/IP EEM does not act as a functional axis of rotation, but rather as a transmission hub and torque transducer for the locally displaced actuation of F/E movements of the T-MCP and T-IP joints, in the same manner that the I-IP EEM transmits and measures the actuation of the I-IP joints from its mounted position on the palm dorsum.

In HX-β, both thumb adduction/abduction (A/A) and circumduction are actuated by the synergistic action of two revolute joints (T-CMC #1 and #2) with axes incident at the thumb CMC joint, the natural center of thumb base movement. To ensure that the virtual axis of circumduction is properly placed and anatomically aligned, HX-β incorporates a setscrew mechanism that enables manual adjustment of the angular offset between the two T-CMC axes. By adjusting the two T-CMC axes to intersect at the anatomical CMC joint in the base of the palm, the HX-β kinematic design enables naturalistic movement and simplified, purely rotational kinematic mapping of thumb base articulation.

2.4.2. Thumb base articulation–carpo-metacarpal (CMC) joint

The workspace of the HX-β PTKC (Fig. 7) can be mapped and navigated using two constituent movement components: adduction/abduction (A/A), and circumduction about the primary axis of the index finger. Thumb A/A is described anatomically as the movement of the thumb's primary axis (T) toward or away from the primary axis (X) of the index metacarpal bone [34] (namely the X axis of HX-β's global reference frame, a palm-fixed Cartesian frame with its origin at the index CMC joint (Fig. 5). Accordingly, the A/A angle, θ_{AA}, may be mathematically defined as:

$$\theta_{AA} = acos\left(\frac{X_{EE}}{\sqrt{{X_{EE}}^2 + {Y_{EE}}^2 + {Z_{EE}}^2}}\right), \quad (1)$$

where X_{EE}, Y_{EE}, and Z_{EE} are the Cartesian coordinates of the PTKC end point (anatomically, the thumb MCP joint) in the global reference frame. Thumb circumduction is described as a circular procession of the thumb (originating from the metacarpal bone) around a variable axis loosely corresponding to the primary axis of the index finger [31]. Using this approximation, we define the circumduction angle θ_C as the angular deviation of the thumb metacarpal from the palmar (XY) plane, as projected onto transverse (ZY) plane (Fig. 5).

With respect to the Cartesian global frame, the circumduction angle can thus be expressed as:

$$\theta_C = acos\left(\frac{Y_{EE}}{\sqrt{{Z_{EE}}^2 + {Y_{EE}}^2}}\right) \quad (2)$$

To effect the constituent functional movements of thumb A/A and circumduction, the PTKC employs synergistic activation of actuation units T-CMC-1 and T-CMC-2, which provide a unique (but not orthogonal) basis for both Cartesian and anatomical space. That is, by virtue of their incident but non-orthogonal axes, each of the T-CMC actuators effects a linear superposition of A/A and circumduction movement components in such a way that enables deterministic navigation of the thumb base workspace. Significantly, because both of the robotic T-CMC axes as well as the axes of thumb A/A and circumduction are all incident at T-CMC joint (approximating its location as equal to the I-CMC joint), the transformation matrix of the PTKC is purely rotational, with the exception of the single link length d_3 – thus greatly simplifying the kinematic computations and facilitating stable control.

The articulation of the palm-thumb kinematic chain, providing the mapping from robot joint space into Cartesian space, is described by the Denavit-Hartenberg (D-H) parameters in Table 1. The mapping of D-H parameters onto the HX-β orthosis is illustrated in Fig. 5b. According to standard convention, the D-H parameters are defined as d (offset along previous "Z axis" of rotation to the common normal), θ (angle about previous z, from old x to new x), r (length of the common normal, in the case of revolute joints, this is the radius about z), α (angle about common normal, from old z axis to new z axis). In this case, as the joint axes are all incident within the T-CMC joint, the only parameters needed to describe the kinematic chain are θ and α and the last d offset. By combining the D-H kinematics with Eqs. (1) and 2, the HX-β robotic joints can be further mapped into anatomical space (described by θ_{AA} and θ_C). The full D-H expression of PTKC "end effector" (T-MCP) is provided in the Appendix.

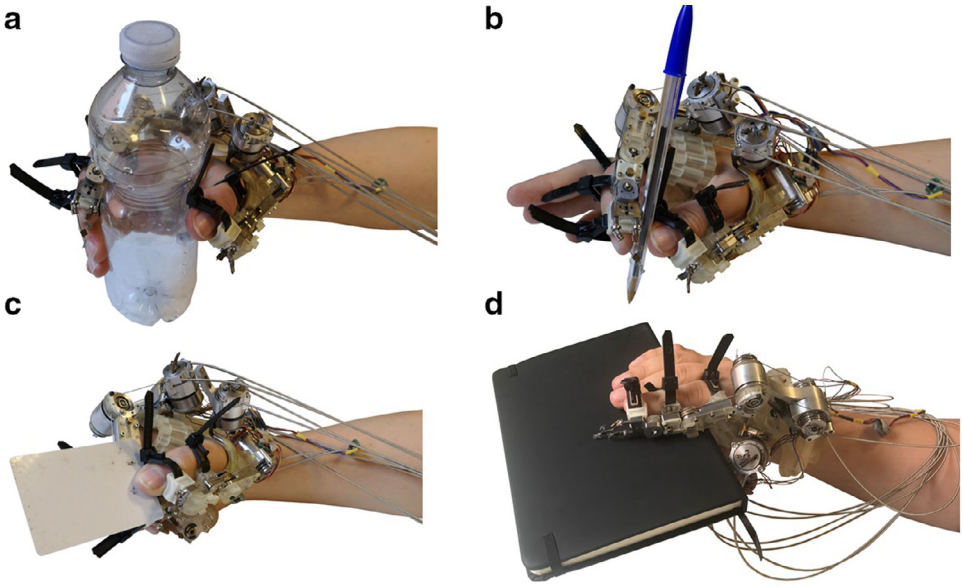

Fig. 6. Grasp Configurations actuated by HandeXos Beta exoskeleton: a) power grasp b) precision pinch grasp c) lateral pinch grasp, and d) palmar grasp.

Table 1
Denavit-Hartenberg parameters.

i	α	r	d	θ
$O_o \sim O_0$		0	0	θ_0
$O_0 \sim O_1$	α_1	0	0	θ_1
$O_1 \sim O_2$	α_2	0	0	θ_2
$O_2 \sim O_3$	0	0	d_3	0

Denavit-Hartenberg variables describing the thumb palm-thumb kinematic chain. α_i is the rotation angle around the x_i axis; $r_i$is the distance between O_i and O_{i+1}, d is the distance along the z_i axis between O_i and O_{i+1}, and θ_i is the angle around the z_i axis.
r_i and d_3 are constant, and determined by the mechanical structure of the device, while θ_i are variables.

Of note, the passive degrees of freedom of the HX-β do not factor into the PTKC kinematics because they act only on the downstream thumb F/E chain (joints T-MCP and T-IP), in series with the PTKC, as well as on the index chain.

2.4.3. HX-β grasp configurations

Functionally, the thumb A/A and circumduction movements actuated by HX-β combine to enable the workspace pictured in Fig. 5, which allows movement of T-MCP joint throughout a wide range of locations with respect to the palm and index finger. This expanded spatial workspace translates to an increased variety of grip configurations that can be actuated with the HX-β, including the lateral pinch grip, precision pinch grip, and modified power grip, illustrated in Fig. 6. With the addition of an another F/E chain to actuate the lateral digits of the hand, the PTKC presents the potential to effect a wider array of full-hand grip configurations, which is the subject of further development for the next-generation HandeXos device.

2.5. HandeXos Beta control architecture

The HX-β system employs a hierarchical control architecture, based on a low-level control scheme (Fig. 7) comprising two alternate modalities, representing two distinct modes of operation – a position-controlled mode, for the performance of 'robot-in-charge' exercises, and a torque-controlled mode, for 'patient-in-charge' training. The inputs to the low-level controllers (desired position or torque, respectively) are provided by the high-level control schemes described in the following subsections, for the position- and torque-control modes.

When in robot-in-charge mode, HX-β effects movements of defined spatiotemporal trajectories, irrespective of joint torque, which is measured in real time via the SEA architecture (EEM). This real-time torque measurement can be used both to quantify the user's joint stiffness, and also to maintain the delivered torque within a pre-defined safety threshold. When in patient-in-charge mode, the motor output (position) is modulated as necessary to achieve the desired output torque, independently of position – with position measured concurrently via the motor-embedded encoders. Thus, in both modes, the HX-β's SEA architecture allows the system to measure the real-time joint positions and delivered torques simultaneously, which may be used both for the evaluation of control system performance, and for assessment of user mobility and function in a variety of rehabilitation exercises.

With respect to hardware and specifications, the low-level controller runs on the FPGA component at 1 KHz, and the high-level controller runs on the robot's real-time processor at 100 Hz – all contained in the bench-top control and actuation unit. At the low level, both the position and torque-control modes operate using an independent PID joint control strategy, wherein the controller for each actuator (corresponding to one joint or one under-actuated joint pair) is tuned independently, and interaction effects between joints are treated as normal disturbances. For all joints and control modes, the output of the PID module (Fig. 7) is fed to a driver (RHOM H bridge driver, 36 V) that calculates and provides the required drive current to the actuators (motors). At the driver level, the actuators are position-controlled via a pulse-width-modulated (PWM) signal and custom-made servo amplifier. The PWM has a fixed frequency of 20 kHz, running on the FPGA level, resulting in 800 duty-cycle discrete levels. In both position and torque control modes, the driver outputs a desired PWM duty-cycle value (expressed in discrete values, from 0 to 800).

The high- and low-level control schemes implemented in the HX-β system are described below, for both position- and torque-control modes. For both control modes, the HX-β's low-level control architecture is compatible with a wide range of additional high-level control strategies that may be developed and implemented in the future, to dynamically adapt to the user's functional capabilities and clinical needs, and thus to optimize rehabilitation outcomes.

2.5.1. Position control mode

In position control (robot-in-charge) mode, at the high level, HX-β has been designed to effect movements along pre-defined spatiotemporal reference angle trajectories, characterized by sigmoidal joint angle

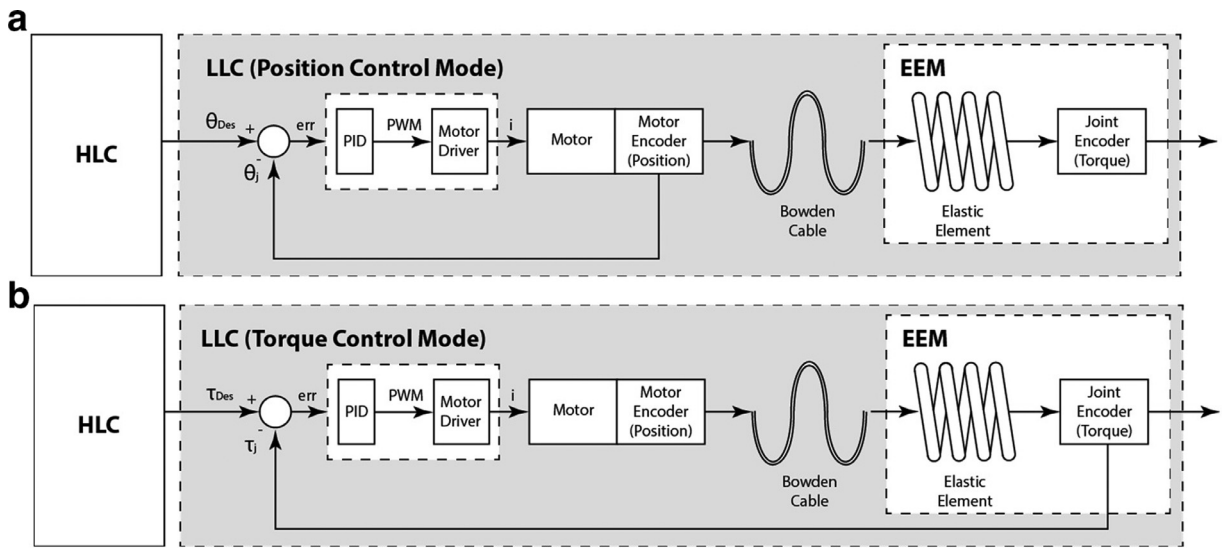

Fig. 7. HandeXos-β Low-Level Closed-Loop Control Architecture for (a) position control mode, and (b) torque control mode.

functions that connect two desired endpoints (positions), with the maximum angular velocities and endpoint positions definable and adjustable by the operator. At the low level, the closed-loop joint position control of each actuator employs a PID regulator operating on the error between the desired position θ_{des} and the measured position θ_{meas} of the motor, as described above (Fig. 7).

Notably, while each SEA unit (active DOF) is independently controlled, the trajectory endpoints for a given exercise/task, corresponding to the "open" and "closed" hand positions, may be defined and effected for all joints simultaneously, thus allowing rapid, patient-customized definition of a range of functional grip configurations. These configurations (including the corresponding ranges of motion to be performed) may be defined with manual assistance from the therapist, as necessary based on the individual needs of the user (patient).

The position control mode may be used both for passive joint mobilization in patients with high spasticity and/or contracted joints, and for training of functional joint coordination patterns. Though it was envisioned initially for users with severe motor impairments and minimal volitional movement ability, robot-in-charge mode may be used as well as for initial training of desired grasping coordination patterns for users across a range of abilities.

2.5.2. Torque control mode

For users with greater volitional movement capabilities, the torque-control (patient-in-charge) mode is indicated. The high-level controller for this mode provides assistive torque according to the *assist-as-need* strategy reported in [35], with torque proportional to the real-time position error between the target and actual joint angle trajectories. In this mode, HX-β orthosis initially exhibits low-impedance behavior, allowing the user to initiate and follow desired movement trajectories with minimal resistance. As in position-control mode, each SEA unit is independently controlled. At the low level, the closed-loop torque control also employs a PID regulator, operating on the error between the desired torque τ_{des} and the actual torque τ_{meas}, calculated as the spring deflection measured by the EEM encoders on the joints multiplied for the spring stiffness.

2.5.3. Graphical user interface (GUI)

A LabVIEW-based graphical user interface (GUI) was developed to allow the HandeXos operator (e.g. physiotherapist or clinical technician) to operate the HX-β system in a simple and efficient manner. The GUI allows selection of the desired control mode (robot vs. patient-in-charge) and rehabilitation exercise, setting and adjusting the controller parameters, viewing desired and measured angles and torques in real-time, and saving/exporting data. The GUI is implemented in LabView (National Instruments, Austin, TX, USA) and runs on the sbRIO Real-Time layer. The GUI features the ability to save combinations of joint positions corresponding to functional grasp configurations, and/or to the limits of an individual user's clinically desirable range of motion). This customization feature allows the operator to customize both the specific grip configuration and the desired range of motion to each individual user, a function which is clinically indespensible. In the clinical use case of patient-in-charge exercises, the target and actual joint trajectories are displayed to users (patients) in real time on a separate screen from the primary GUI.

3. Methods-HandeXos Beta performance characterization

To evaluate the essential performance of the HandeXos Beta system, a series of physical performance characterizations were performed on the index kinematic chain, including the I-MCP, I-PIP, and I-DIP joints. In addition to step and chirp response characterizations of the low-level controllers for both position and torque control modes, the HX-β end effector output forces were characterized at the robotic fingertip, and output impedance in transparent (zero-torque) mode was measured during both externally applied stereotyped movements and during device use by a healthy subject.

3.1. Experimental configuration and test fixture

To characterize the I-MCP, I-PIP, and I-DIP joints, the HX-β index module was mounted in a custom-built test fixture, in a fully extended position, oriented so that joint flexion and extension were effected in the horizontal plane, independently of gravitational forces. A load cell (Futek model LSM400 Mini Beam Load Cell) was placed in contact with the terminal end effector, to measure the force exerted at the robotic fingertip, perpendicular to the finger's primary axis. To isolate and verify the performance of each individual joint, two custom aluminum splints were applied across the I-DIP and I-PIP joints (respectively), which act together as a single under-actuated pair during normal HX-β operation. Likewise, the test fixture featured a removable bracket allowing the I-MCP joint to be locked in place, so that separate characterizations could be performed for each individual joint. Isolating the movement of each joint in this way enabled the direct assessment of the essential performance of the low-level controllers and joint mechanics under ideal con-

ditions of maximum stability, free from gravity and from dynamic multi-joint interactions anticipated during typical use.

3.2. Low-level controller performance characterization

The dynamic closed-loop behavior of the low-level controllers for both the position- and torque-control modes was characterized by analyzing the response of the system to step and chirp reference signals, under unloaded conditions. For the position control step responses, 20 repetitions of 60° step displacements were performed for both flexion and extension of the I-MCP, I-PIP and I-DIP joints, respectively. For the position control chirp response, the initial (target) range of motion was set to ±20°, with a frequency range of 0.1–5 Hz and a total duration of 150 s.

For the closed-loop torque control step response, data were collected for 20 repetitions of 0–0.1 N·m flexion torque step input for the I-MCP, I-PIP and I-DIP joints. The magnitude of this torque step was approximately one third of the dynamic range actuated by HX-β during typical use, and was chosen to represent the magnitude of a foreseeably high instantaneous torque control command in the context of error-based assistance, as implemented in patient-in-charge mode. Chirp response experiments were performed at a magnitude of 0.1 N·m, with a frequency range of 0.1–5 Hz and a total duration of 150 s.

For both position and torque control modes, the tuning of the low-level control PID parameters was done empirically, due to the inability to accurately model the variable friction in the cable-sheath transmission lines [25]. In order to minimize the variability between the tuning conditions and application conditions, tuning was performed with a healthy subject wearing the HX-β orthosis, with a system configuration and layout closely reflecting the intended use scenario, with the bench-top system modules placed on a desk beside the subject, and cable curvature minimized.

3.3. Exerted force at the fingertip

The force exerted by the HX-β end effector was measured via mono-axial load cell at the tip of the robotic finger. The force was measured while imposing a torque of 0.3 N·m on each index joint. The lengths the finger segments were 42 mm for the proximal phalanx, 28 mm for the middle phalanx, and 16 mm for the distal phalanx.

3.4. Output impedance characterization in stereotyped movements

To evaluate the functional effectiveness of the torque control mode under simulated conditions of use, the output impedance of the HX-β orthosis – representing the residual stiffness felt by the user – was measured in transparent mode (i.e. torque control mode, with a target output torque of 0 N·m), during both externally applied F/E movements, and during device use by a healthy user. Initially, the single-joint output impedance was measured individually for the I-MCP, I-PIP, and I-DIP joints, with the HX-β index module in the test fixture. This was achieved by restraining two joints at a time with a rigid metal link, while leaving the joint of interest free to move. Stereotyped movements were externally imposed on the device, consisting of cyclic F/E repetitions with an approximate range of motion of 0–60° of flexion and a frequency content in the range between 0.1 and 2 Hz. Movement was applied manually, using a metronome to modulate frequency. Output impedance was computed and represented in the form of Bode plots (Fig. 10), by transforming the simultaneous joint position-torque time series recorded in transparent mode into the frequency domain and normalizing the torque magnitude by natural spring stiffness of 1.34 N·m/rad, which represents the effective stiffness felt by the user due to the compliance of the EEM when the motors are locked.

Table 2
Position-control mode characterization.

Joint	Movement	Rise time[s]	Overshoot[°]
I-MCP	Flexion	0.334 ± 0.001	0.013 ± 0.010
	Extension	0.335 ± 0.001	< 0
I-PIP	Flexion	0.322 ± 0.001	0.013 ± 0.010
	Extension	0.321 ± 0.001	0.033 ± 0.019
I-DIP	Flexion	0.413 ± 0.001	0.002 ± 0.003
	Extension	0.414 ± 0.001	0.033 ± 0.019

Rise times and overshoots for the position-control step responses of the three joints (I-MCP, I-PIP, I-DIP) – reported as mean ± std. deviation. Rise time defined as time to reach 98% of the target value. Conditions exhibiting no (i.e. negative) overshoot denoted as "< 0".

3.5. Output impedance in functional tasks

Following the single-joint impedance characterizations, the functional output impedance of the entire HX-β device (including simultaneous movement of all joints) was evaluated in transparent mode on a healthy user performing functional grasps of various configurations, under their own volition. During this characterization, the orthosis was worn by a healthy subject, who was instructed to grasp a series of reference objects (Fig. 6) with the reference of a metronome, at increasing frequency, within the range of 0.1–2 Hz, for a total of 20 grasp repetitions per configuration/object.

Simultaneous position and torque profiles were recorded for each SEA unit, and the output impedance function was then calculated with the residual output torque normalized by the spring natural stiffness, in the same manner as for the stereotyped movements. By requiring continuous rejection of random disturbances on all joints simultaneously throughout a repeated functional grasping task, this test served as an integrated evaluation of system-level performance, including the anatomical suitability and proper adjustment of the HX-β kinematic architecture, the function of the series-elastic actuator architecture (including sensing, actuation, and transmission elements), and the performance of the low-level torque controllers.

4. Results

4.1. Control system performance characterization

4.1.1. Position control characterization

The average position step responses for the three joints (I-MCP, I-PIP and I-DIP) are shown in Fig. 9a for both flexion (−30°–30°) and extension (30°–30°), with corresponding rise times and overshoots reported in Table 2. On average, rise times in both flexion and extension steps were approximately 0.33 s for I-MCP, 0.32 s for I-PIP, and 0.41 s for I-DIP. Overshoots, when present, were always lower than 0.02° Fig. 9b displays the first 15 s and the last 2 s of the chirp responses, and Fig. 9c presents the corresponding Bode diagrams. All joints exhibited excellent signal tracking for the first 15 s (freq. range 0.1–0.5 Hz) of the chirp response, with −3 dB cut-off frequencies of 2.63 Hz for I-MCP and 2.72 Hz for both I-PIP and I-DIP.

4.1.2. Torque control characterization

Average profiles for the torque step response of the three joints are shown in Fig. 8a, with corresponding rise times and overshoots reported in Table 3. On average, rise times in flexion steps were approximately 0.20 s for I-MCP and 0.30 s for both I-PIP and I-DIP, all with overshoots in the range of 0–0.001 Nm. Fig. 8b displays the first 15 s and the last 2 s of the chirp responses, and Fig. 8c presents the corresponding Bode diagrams. As in position control mode, all joints exhibited excellent signal tracking for the first 15 s (freq. range 0.1–0.5 Hz) of the chirp response,

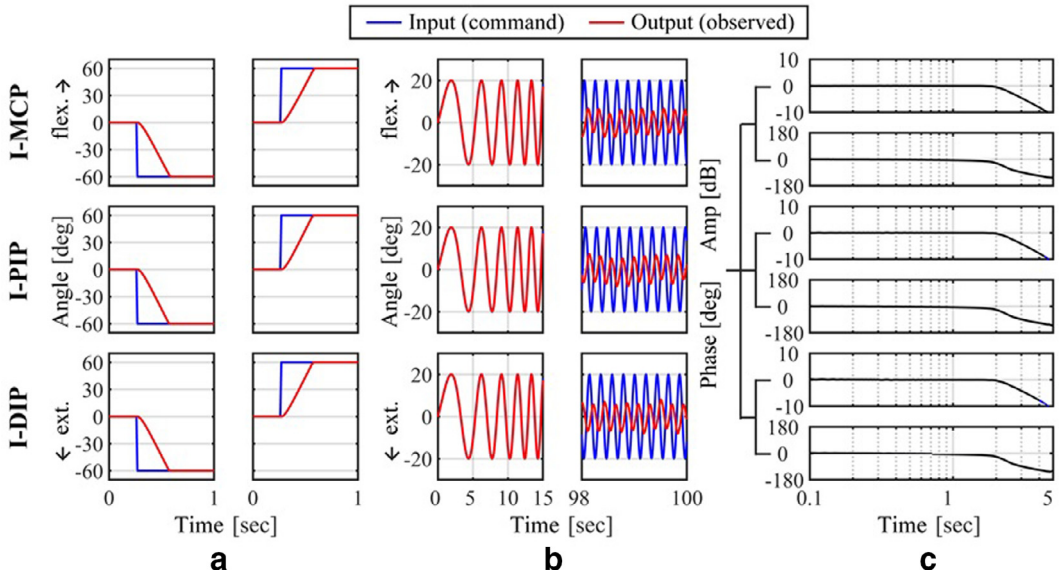

Fig. 8. HX-β torque control performance for the three index joints: (a) step response in flexion, (b) chirp response for the first fifteen seconds (left) and the last two seconds (right), (c) Bode diagrams of amplitude (top) and phase (bottom) of the chirp response output relative to input.

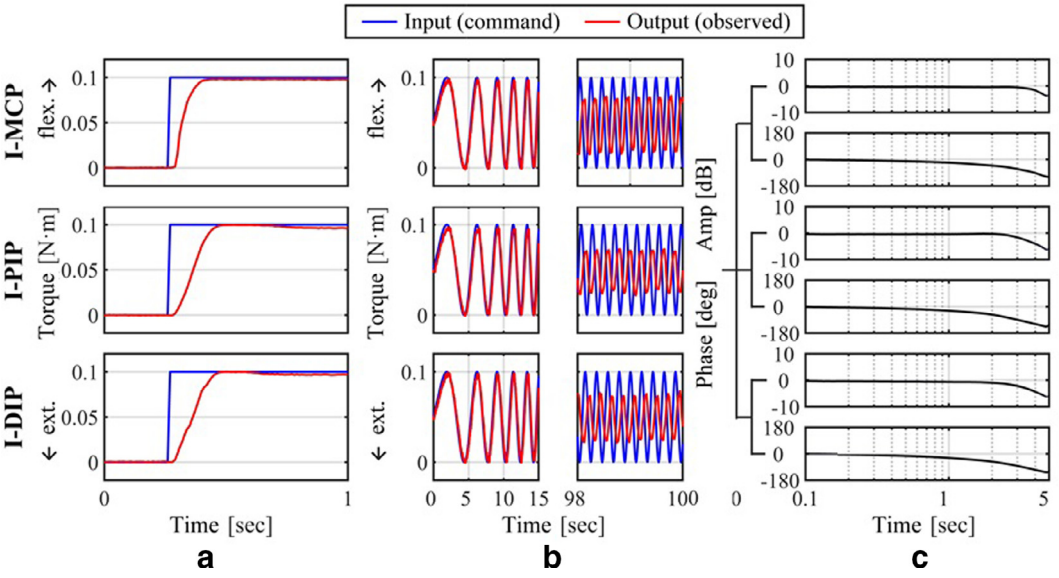

Fig. 9. HX-β performance characterization in position control mode, for the three index module (I-) joints – metacarpophalangeal (MCP), proximal interphalangeal (PIP), and distal interphalangeal (DIP): (a) step response in extension (left) and flexion (right), (b) chirp response for the first fifteen seconds (left) and the last two seconds (right), (c) Bode diagram amplitude (top) and phase (bottom) of the chirp response output relative to input.

Table 3
Torque mode characterization.

Joint	Movement	Rising time[s]	Overshoot[°]
I-MCP	Flexion	0.197 ± 0.054	< 0
I-PIP	Flexion	0.306 ± 0.018	0.001 ± 0.001
I-DIP	Flexion	0.303 ± 0.008	0.001 ± 0.001

Rise times and overshoots for the torque-control step responses of the three joints (I-MCP, I-PIP, I-DIP) – reported as mean ± std. deviation. Rise time defined as time to reach 98% of the target value. Conditions exhibiting no (i.e. negative) overshoot denoted as "< 0".

with −3 dB cut-off frequencies of 4.01 Hz for I-MCP, 4.12 Hz for I-PIP, and 2.55 Hz for I-DIP.

4.2. Exerted force at the fingertip

Data were averaged over a period of 5 s, and the offset was subtracted. The exerted forces in ideal conditions would be 4.7 N for the I-MCP joint, 6.81 N for I-PIP, and 18.75 N for I-DIP. Due to friction and overall transmission losses in the cables, the device exerted an actual fingertip force of 4.32 N with the I-MCP joint (91% of the theoretical force), 3.73 N for the I-PIP joint (64% of the theoretical force), and 4.05 N for the I-DIP joint (21% of the theoretical force).

4.3. Output impedance

4.3.1. Index chain output impedance–stereotyped movements

The parasitic output impedances of each index joint (measured in the corresponding EEM), representing the residual joint stiffness felt by the user with the HX-β in transparent mode, are represented as Bode plots in

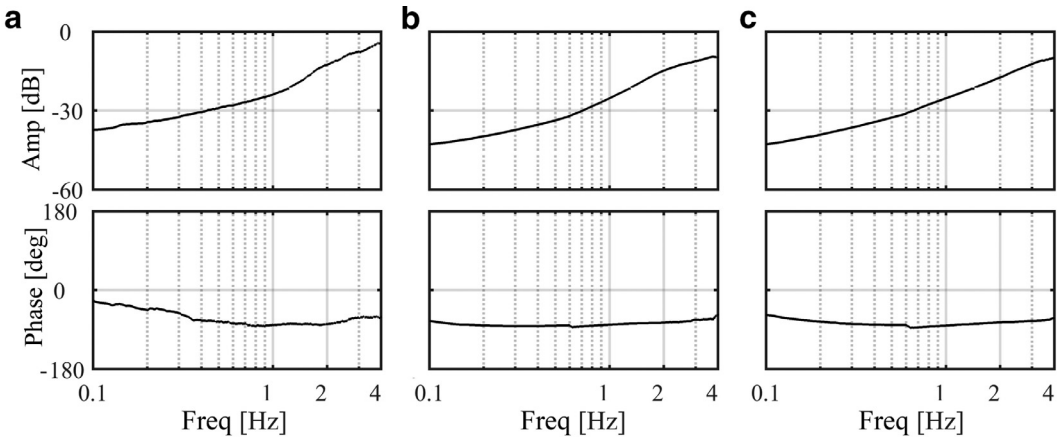

Fig. 10. Bode plots of the amplitude and phase lag of the parasitic joint output impedance (residual stiffness) for externally applied stereotyped movements in transparent mode, normalized with respect to the natural spring stiffness (1.34 N·m/rad), for (a) I-MCP joint; (b) I-PIP joint; (c) I-DIP joint.

Table 4
Joint output impedance – functional grasps in transparent mode (dB).

Joint (EEM)	Lateral grasp	Palmar grasp	Pinch grasp	Power grasp	Average
I-MCP	−23.13	−24.50	−23.44	−22.35	−23.36
I-IP	−26.34	−28.28	−26.18	−28.69	−27.37
T-CMC#1	−14.88	−11.45	−13.87	−20.08	−15.07
T-CMC#2	−22.91	−12.19	−15.67	−21.77	−18.14
T-MCPIP	−11.45	−10.58	−16.07	−15.10	−13.30

Output impedance at 1 Hz for all HX-β actuation units (EEMs) during voluntary performance of functional grasps. Impedance reported in dB, relative to natural EEM spring stiffness of 1.34 N·m/rad.

Fig. 10. For the I-MCP joint, the stiffness felt by the user with the HX-β in transparent mode, are represented as Bode plots in Fig. 10. For the I-MCP joint, the parasitic impedance up to 0.5 Hz is −29 dB relative to the natural spring constant, which corresponds to an absolute value of 0.048 N·m/rad. This means that while in transparent mode, the system presents a stiffness which is about 28 times smaller than the natural spring stiffness during low-frequency movements. As the user increases the movement frequency, the parasitic impedance value increases, up to −24 dB at 1 Hz (0.085 N·m/rad), and −13 dB at 2 Hz (0.30 N·m/rad).

For the I-PIP joint, the normalized parasitic stiffness up to 0.5 Hz is −34 dB, corresponding to an absolute value of 0.027 N·m/rad – about 50 times smaller than the natural spring stiffness. As the user increases the joint movement frequency, the parasitic impedance value increases, up to −25 dB at 1 Hz (0.075 N·m/rad), and −15 0 dB at 2 Hz (0.24 N·m/rad). For I-DIP, the normalized parasitic stiffness up to 0.5 Hz is −33 dB, corresponding to an absolute value of 0.030 N·m/rad – about 45 times smaller than the natural spring stiffness. The parasitic impedance increases to −25 dB at 1 Hz (0.075 N·m/rad) and −17 dB at 2 Hz (0.19 N·m/rad).

4.3.2. *Full hand output impedance–functional grasping*

The output impedance for each EEM (each representing one joint or co-actuated joint pair) calculated in transparent mode during the voluntary execution of functional grasps is shown in Fig. 11, with results of the corresponding frequency analysis summarized in Table 4.

5. Discussion

In wearable rehabilitation robots, the ability to precisely measure and modulate externally applied joint torques in real time is paramount to implementing error-based assistance paradigms that assist users on an as-needed basis and thus facilitate continuous progress in functional rehabilitation. Through its novel series-elastic actuator (SEA) architecture, the HandeXos Beta hand exoskeleton provides precisely this closed-loop torque modulation functionality, and the present study demonstrates the HX-β system's essential performance in several key capacities supporting this functionality. With respect to control system performance, functionally appropriate step responses were achieved for both position and torque control modes, including reasonably low settling times, on the order of 0.2–0.4 s, and overshoots in the range of 0.001°. As well, the position and torque control bandwidths, with cutoff frequencies ranging from 2.5 Hz to upwards of 4 Hz, were comfortably high enough to facilitate typical rehabilitation protocols, which are usually performed in a frequency range of approximately 1 Hz ([36–38]).

By comparison to previously reported hand exoskeletons, the HX-β's lowest torque bandwidth of 2.55 Hz, achieved at the I-DIP joint, was comparable to the 2.50 Hz bandwidth reported by a previous index finger exoskeleton developed by Agarwal et al. [27], despite the overall higher weight of the HX-β orthosis (~420 g vs. 80 g, due to the HX-β SEA architecture and additional thumb module). As a safety measure to prevent cable breakage, the present version of the HX-β exoskeleton was set to operate within a maximum torque range of approximately ±0.5 N·m per joint, as necessary given the limited tensile strength and inherent frictional losses of the Bowden transmission cables. This maximum torque value is relatively low compared to those reported by other hand exoskeletons [2,39], but still comparable to physiological torque values [40], and thus adequate to assist in the execution of functional activities for users with limited joint stiffness some residual hand function. As well, the HX-β device has demonstrated the ability to exert functionally relevant fingertip forces on the order of 4 N, relative to the physiological standard of 5.7 N [40]. Nonetheless, to address this performance limitation and enable more effective treatment of spastic or otherwise stiff hands, the maximum output torque is currently being increased in subsequent HX iterations, via appropriate specification of transmission cables, adequately powered brushless DC motors, and kinematic refinements to streamline the cable routing.

Another limitation of the HX-β architecture is the imprecision of joint angle measurements resulting from a combination of factors. The first is the separation within each SEA unit between the active exoskele-

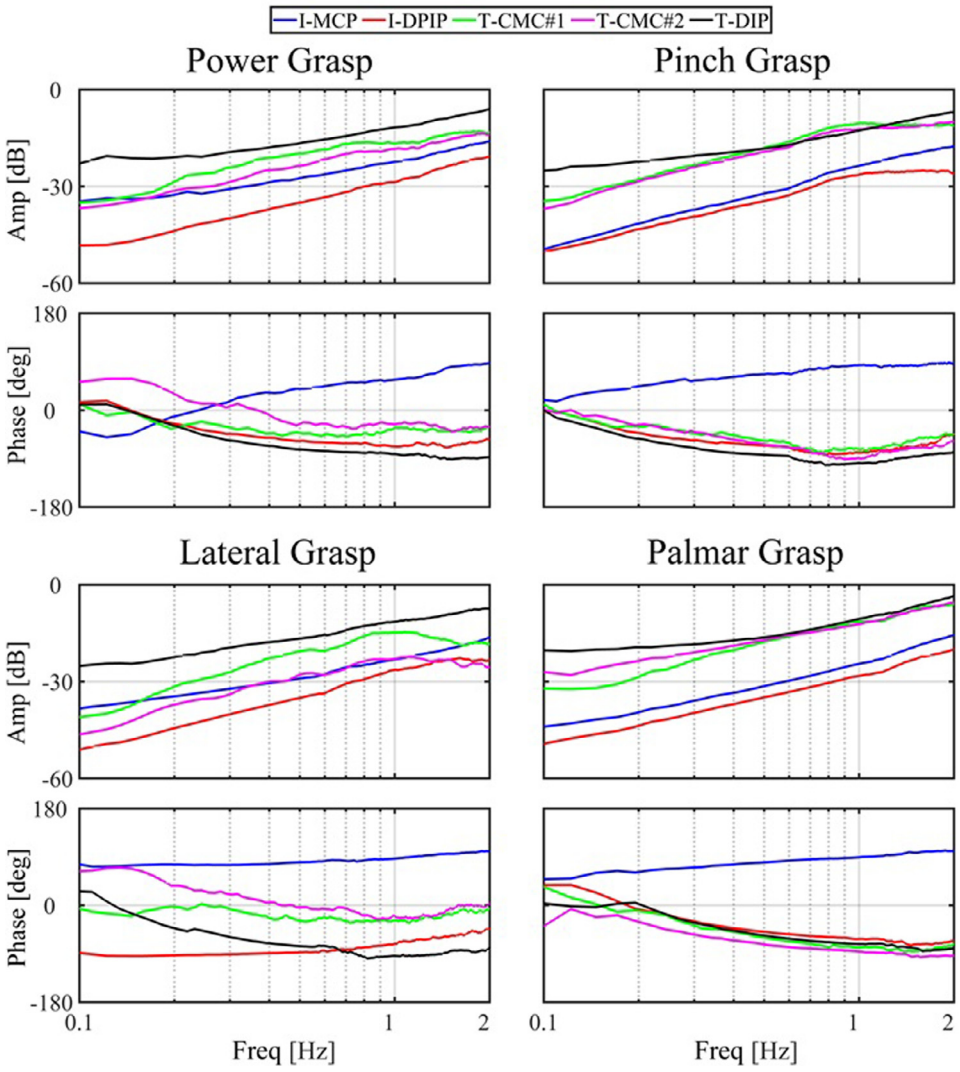

Fig. 11. Bode plot of amplitude and phase lag of the parasitic joint output impedance of all the joints of the HX-β exoskeleton, normalized to the natural SEA- EEM spring stiffness (1.34 N·m/rad), during voluntary grasping in transparent mode, for (a) power grasp; (b) pinch grasp; (c) lateral grasp; (d) palmar grasp.

ton joints and the motor encoders used to estimate joint displacement, which are located in the bench-top actuation unit control unit (Fig. 1), separated by transmission cables with variable effective elasticity and friction. Meanwhile, the EEMs integrated into the exoskeleton and coupled directly to their corresponding joints are each equipped with a single encoder used to measure delivered torque (via torsional spring deformation), but not the absolute joint angle. Furthermore, the kinematic relationships between each SEA unit's displacement and the corresponding anatomic joint angles are not rigidly defined, and subject to variations in user hand size and fitting. Finally, there remains an addition level of joint angle indeterminism in the inter-phalangeal (IP) SEA units, due to the coupled under-actuation of the index IP joints and thumb MCP and IP joints, but this can be recovered from the true joint angle encoders integrated into the passive joints (Fig. 3). In practice, the cumulative uncertainty in true joint angle control and measurement can be mitigated with an appropriate calibration procedure and corresponding software, allowing reference positions to be defined and recorded by the user and/or operator, based on the measured encoder values corresponding to known grasp configurations of a series of reference objects (effected with manual assistance from the therapist, as necessary). By interpolating between the manually-defined "open" and "closed" grasp configurations, the HX-β can thus achieve a clinically adequate degree of position control within the functional range of motion defined for each exercise/task.

A limitation of the present study was the isolation of component-level performance characterizations to the index kinematic chain, with performance evaluation of the thumb kinematic chain conducted only at the integrated system level, in the context of effecting functional grasp configurations and measuring output impedance during functional grasps. This two-pronged approach to performance characterization was strategically designed to span a wide spectrum of system performance aspects, from a rigorous assessment of single-joint mechanics and control system behavior in an ideally controlled test fixture (facilitated by the single-plane articulation of the index chain), to functionally integrated demonstrations of full system performance. Regarding the effectiveness of HX-β's novel kinematic architecture, the functional grasps depicted in Fig. 6 demonstrate the capacity of the HX-β robotic orthosis to actuate a variety of functionally relevant grasp configurations uniquely enabled by the articulation of the palm-thumb kinematic chain. Further, the finding of suitably low residual output impedance in all active SEA units throughout a full range of natural grasping activities performed at life-like speeds (~1 Hz) with the system in transparent mode demonstrates both the kinematic suitability of the HX-β to the functional anatomy of the hand, and the system-level performance of the SEA-enabled torque control system to continually sense and accurately modulate externally transferred torque in real time.

6. Conclusion

This work presents the mechatronic design and essential performance characterization of HandeXos Beta, a novel self-aligning index-thumb exoskeleton for hand rehabilitation. HX-β's primary innovations include a novel kinematic chain for dexterous thumb articulation, a unique series-elastic actuator (SEA) architecture for directly controlled modulation of output torque, and a series of ergonomic adjustment and self-alignment mechanisms. In addition to ensuring a mechanically compliant and inherently safe interaction with the user's hand, the SEA-enabled torque control mode allows for the implementation of adaptive, progressive rehabilitation exercise paradigms that provide movement assistance on an as-needed basis. While the compact size and moderately light weight of the HX-β orthosis minimize its net encumbrance, its adjustability and self-alignment mechanisms maximize HX-β's clinical utility and adaptability to a wide range of users.

In sum, the set of performance characterizations in the present study confirm that HandeXos Beta's kinematic design confers a functionally significant improvement in the variety of actuated grip configurations – and further, that the HX-β overall system performance is stable, responsive, adequately powerful, and conducive to natural functional grasping movements, thus rendering it well-suited to clinical application. Accordingly, future works will aim at extending the HX-β architecture to a full-hand version, and at conducting human clinical studies to assess the safety, feasibility, and effectiveness of the HandeXos platform as a tool for neurological hand rehabilitation.

Declaration of interest

The authors declare that they have no known competing financial interests or personal relationships that could have appeared to influence the work reported in this paper.

Supplementary material

Supplementary material associated with this article can be found, in the online version, at doi:10.1016/j.mechatronics.2019.06.001.

References

[1] Heo P, Gu GM, jin Lee S, Rhee K, Kim J. Current hand exoskeleton technologies for rehabilitation and assistive engineering. *Int J Precis Eng Manuf* 2012;13(5):807–24.
[2] Schabowsky LPS, CN, Godfrey SB, Holley RJ. Development and pilot testing of HEXORR: hand. *J Neuroeng Rehabil* 2010;7(36):1–16.
[3] Brokaw EB, Black I, Holley RJ, Lum PS. Hand spring operated movement enhancer (HandSOME): a portable, passive hand Exoskeleton for stroke rehabilitation. *IEEE Trans Neural Syst Rehabil Eng* 2011;19(4):391–9.
[4] Soekadar SR, et al. Hybrid EEG/EOG-based brain/neural hand exoskeleton restores fully independent daily living activities after quadriplegia. *Sci Robot* 2016;1(1):eaag3296.
[5] Witkowski M, Cortese M, Cempini M, Mellinger J, Vitiello N, Soekadar SR. Enhancing brain-machine interface (BMI) control of a hand exoskeleton using electrooculography (EOG). *J Neuroeng Rehabil* 2014;11(1):1–6.
[6] Lucas L, Dicicco M, Matsuoka Y. An EMG-controlled hand exoskeleton for natural pinching. *J Robot Mechatronics* 2004;16(5):1–7.
[7] Vitiello N, et al. NEUROExos: a powered elbow exoskeleton for physical rehabilitation. *IEEE Trans Robot* 2013;29(1):220–35.
[8] Cortese M, Cempini M, De Almeida Ribeiro PR, Soekadar SR, Carrozza MC, Vitiello N. A mechatronic system for robot-mediated hand telerehabilitation. *IEEE/ASME Trans Mechatronics* 2015;20(4):1753–64.
[9] Vitiello N, et al. Functional design of a powered elbow orthosis toward its clinical employment. *IEEE/ASME Trans Mechatronics* 2016;21(4):1880–91.
[10] Lum PS, Burgar CG, Shor PC, Majmundar M, Van der Loos M. Robot-assisted movement training compared with conventional therapy techniques for the rehabilitation of upper-limb motor function after stroke. *Arch Phys Med Rehabil* 2002;83(7):952–9.
[11] Tomić TJD, et al. ArmAssist robotic system versus matched conventional therapy for poststroke upper limb rehabilitation: a randomized clinical trial. *Biomed Res Int* 2017;2017.
[12] Kwakkel G, Kollen BJ, Krebs HI. Effects of robot-assisted therapy on upper limb recovery after stroke: a systematic review. *Neurorehabil Neural Repair* 2008;22(2):111–21.
[13] Krebs HI, Hogan N, Aisen ML, Volpe BT. Robot-aided neurorehabilitation. *IEEE Trans Rehabil Eng* 1998;6(1):75–87.
[14] Lo AC, et al. Robot-assisted therapy for long-term upper-limb impairment after stroke. *N Engl J Med* 2010;362(19):1772–83.
[15] Anderson KD. Targeting recovery: priorities of the spinal cord-injured population. *J Neurotrauma* Oct. 2004;21(10):1371–83.
[16] Chiri A, et al. HANDEXOS: towards an exoskeleton device for the rehabilitation of the hand. In: 2009 IEEE/RSJ Int. Conf. Intell. Robot. Syst. IROS 2009; 2009. p. 1106–11.
[17] Polygerinos P, et al. Towards a soft pneumatic glove for hand rehabilitation. *IEEE Int Conf Intell Robot Syst* 2013:1512–17.
[18] Polygerinos P, Wang Z, Galloway KC, Wood RJ, Walsh CJ. Soft robotic glove for combined assistance and at-home rehabilitation. *Rob Auton Syst* 2015;73:135–43.
[19] Yap HK, Lim JH, Nasrallah F, Goh JCH, Yeow RCH. A soft exoskeleton for hand assistive and rehabilitation application using pneumatic actuators with variable stiffness. *Proc - IEEE Int Conf Robot Autom* 2015;2015–June(June):4967–72.
[20] Kadowaki Y, Noritsugu T, Takaiwa M, Sasaki D, Kato M. Development of soft power-assist glove and control based on human intent. *J Robot Mechatronics* 2011;23(2):281–91.
[21] Cempini M, Cortese M, Vitiello N. A powered finger-thumb wearable hand exoskeleton with self-aligning joint axes. *IEEE/ASME Trans Mechatronics* 2015;20(2):705–16.
[22] Cempini M, Marzegan A, Rabuffetti M, Cortese M, and Vitiello N. Analysis of relative displacement between the HX wearable robotic exoskeleton and the user's hand Analysis of relative displacement between the HX wearable robotic exoskeleton and the user's hand, 2014.
[23] Stienen H van der K, Arno HA, Edsko EG Hekman, Frans CT van der Helm. Self-aligning exoskeleton axes through decoupling of joint rotations and translationsvol. vol. 25, no.3, pp. 628–633, 2009.
[24] Stienen H van der K, Arno HA, Edsko EG Hekman, Huub ter Braak, Arthur MM Aalsma, Frans CT van der Helm. Design of a rotational hydro-elastic actuator for an active upper-extremity rehabilitation exoskeleton, pp. 881–888, 2008.
[25] Veneman JF, Ekkelenkamp R, Kruidhof R, Van Der Helm FCT, Van Der Kooij H. A series elastic- and Bowden-cable-based actuation system for use as torque actuator in exoskeleton-type robots. *Int J Rob Res* 2006;25(3):261–81.
[26] Pratt GA, Williamson MM. Series elastic actuators. In: Proc. 1995 IEEE/RSJ Int. Conf. Intell. Robot. Syst. Hum. Robot Interact. Coop. Robot., 1; 1995. p. 399–406.
[27] Agarwal P, Fox J, Yun Y, O'Malley MK, Deshpande AD. An index finger exoskeleton with series elastic actuation for rehabilitation: design, control and performance characterization. *Int J Rob Res* 2015;34(14):1747–72.
[28] Jorge AD, Badesa FJ, Blanco A, Garcı N, and Lledo LD. Hand exoskeleton for rehabilitation therapies with integrated optical force sensor, vol. 10, no. 2, pp. 1–11, 2018.
[29] Li Z-M, Tang J. Coordination of thumb joints during opposition. *J Biomech* Jan. 2007;40(3):502–10.
[30] Cooney WP, Linscheid RL, An KN. Opposition of the thumb: an anatomic and biomechanical study of tendon transfers. *J Hand Surg Am* Nov. 1984;9(6):777–86.
[31] Kapandji AI. Clinical evaluation of the thumb' s opposition. *J Hand Ther* 1986;5(2):102–6.
[32] Tsagarakis NG, Laffranchi M, Vanderborght B, Caldwell DG. A compact soft actuator unit for small scale human friendly robots. In: 2009 IEEE Int. Conf. Robot. Autom.; 2009. p. 4356–62.
[33] Baldoni A, Vitiello N, Cempini M, Cortese M, Crea S, Carrozza MC. Mechatronics design and validation of a miniaturized SEA transmission system. Mechatronics 2018;49(May 2017):149–56.
[34] Chao EYS, An K-N, Cooney III WP, and Linscheid RL. Biomechanics of the hand: a basic research study, 1989, p. 191.
[35] Trigili E. Detection of movement onset using EMG signals for upper-limb exoskeletons in reaching tasks. et al 2019;1:1–16.
[36] Tsagarakis NG, Caldwell DG. Development and control of a 'soft-actuated' exoskeleton for use in physiotherapy and training. *Auton Robots* 2003;15(1):21–33.
[37] Frisoli A, Salsedo F, Bergamasco M, Rossi B, Carboncini MC. A force-feedback exoskeleton for upper-limb rehabilitation in virtual reality. *Appl Bionics Biomech* 2009;6(2):115–26.
[38] Nef T, Mihelj M, Riener R. ARMin: a robot for patient-cooperative arm therapy. *Med Biol Eng Comput* 2007;45(9):887–900.
[39] Wege A, Hommel G, and Berlin TU. Development and control of a hand exoskeleton for rehabilitation of hand injuries, no. 1.
[40] Bundhoo V, Park EJ. Design of an artificial muscle actuated finger towards biomimetic prosthetic hands. In: 2005 Int. Conf. Adv. Robot. ICAR '05, Proc., 2005; 2005. p. 368–75.

Dario Marconi is a PhD Student at the Biorobotics Institute of Scuola Superiore Sant'Anna (Pisa).

He received the MSc degree in biomedical engineering from the University of Pisa, Pisa, Italy, in 2015. His research activities include the development of control strategies for robot-assisted hand rehabilitation and the assessment of functional requirement for hand exoskeletons.

Andrea Baldoni received his BSc and MSc in Mechanical Engineering from the University of Perugia in 2011 and 2013, respectively. He is currently a Ph.D. student at The BioRobotics Institute of Scuola Superiore Sant'Anna, Pisa, Italy. His research interests are in the field of mechanical solutions and innovative technologies.

Zach McKinney is a Post-Doctoral Research Fellow at the BioRobotics Institute of Scuola Superiore Sant'Anna (Pisa). He received his bachelor's degree in mechanical engineering from Princeton University (2007), and both his MS (2008) and PhD (2016) in biomedical engineering from the University of California, Los Angeles (UCLA). Throughout this time, he has worked in both academic and commercial settings on the research, development, and clinical validation of neurorehabilitation technologies – most recently, as the chief science officer and co-founder of Spinal Singularity. Zach is currently chairing IEEE's standardization Working Group PAR-2794 to promote greater interoperability among neural interfacing and rehabilitation technologies.

Marco Cempini received the Ph.D. in Robotics at The BioRobotics Institute, Scuola Superiore Sant'Anna, Pisa, Italy, in 2014. His research interest included human-robot physical interaction, and intrinsically safe mechatronics design of actuators and transmissions for wearable robotics, especially for application in assistance/rehabilitation of impaired or weak subjects. He was an original co-founder of the start-up IUVO srl, and he won the 2015 KUKA Innovation Award.

From September 2015 till June 2017, he was a Post-Doctoral fellow at the Shirley Ryan Ability Lab (ex RIC), where he worked on disruptive architectures for lower-limb robotic prostheses, with a greater focus on mechatronics performances and end-users acceptability. His research interest kept focusing on viable designs for human-interactive robotics, especially in healthcare applications. He is currently head of design engineering at Neocis Inc., a start-up providing haptic robotic guidance solutions for precise dental and oral surgery.

Dr. Cempini is the author or co-author of 18 ISI/Scopus journal papers and 15 peer-review conference proceedings papers, and 4 granted and 3 pending patents. He served as a referee for over 22 ISI journals, for more than 50 submissions.

Dr. Simona Crea received her PhD in Biorobotics from Scuola Superiore Sant'Anna on December 2015. Since April 2017 she is an Assistant Professor at The BioRobotics Institute of Scuola Superiore Sant'Anna, where she works on wearable robotics. Her research activities are focused on developing and validating novel wearable technologies and paradigms of human-robot interaction, with a focus on ergonomics and behavioral aspects. She is project manager of the H2020 CYBERLEGs Plus project, and co-PI of two national projects funded by INAIL (the National Institute for Insurance against Accidents at Work), namely the MOTU and Habilis project.

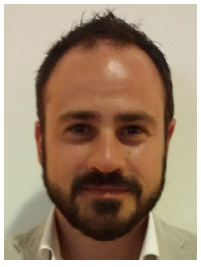

Prof. Nicola Vitiello (M'12) received his MSc degree in Biomedical Engineering (cum laude) from the University of Pisa, Italy, in 2006, and from Scuola Superiore Sant'Anna (SSSA), Pisa, Italy, in 2007. He also received his PhD degree in Biorobotics from SSS in 2010. He is currently an Associate Professor at The BioRobotics Institute, SSSA, where he leads the Wearable Robotics Laboratory. He is the author or co-author of more than 40 ISI/Scopus papers and more than 30 peer-review conference proceedings papers. He is/has been a guest editor of three special issues (SI) in the following ISI journals: Robotics and Autonomous Systems, IEEE Transactions on Neural Systems and Rehabilitation Engineering, and IEEE Robotics and Automation Magazine. He has served as the Scientific Secretary of the EU FP7 CA-RoboCom project, and he was the scientific project coordinator of the EU FP7 CYBERLEGs project and the EARLYREHAB project funded by Regione Toscana. Currently, he is the scientific project coordinator of the IUVO research project funded by a local bank foundation, i.e., "Fondazione Pisa," and partner of the H2020-ICT-AIDE project. His interests include the development, experimental validation and maturation of novel wearable robotic devices for human motion assistance and rehabilitation. On January 2015, together with colleagues, he co-founded the spin-off company IUVO SrL.